Journal of Photochemistry and Photobiology A: Chemistry 213 (2010) 180–188

Contents lists available at ScienceDirect

Journal of Photochemistry and Photobiology A: Chemistry

journal homepage: www.elsevier.com/locate/jphotochem

Theoretical characterizations of electronically excited silaazulene skeletons

Yoshiaki Amatatsu*

Faculty of Engineering and Resource Science, Akita University, Tegata Gakuen-cho, Akita 010-8502, Japan

ARTICLE INFO

Article history:
Received 16 March 2010
Received in revised form 28 May 2010
Accepted 31 May 2010
Available online 8 June 2010

Keywords:
Silaazulene
Azulene
Internal conversion
Ab initio MO calculation
Excited state
Heavier 14 group elements

ABSTRACT

Silaazulene (SIAZ) skeletons where one of the C atoms in the azulene skeleton is replaced by Si atom have been characterized from a viewpoint of the excited state by means of ab initio complete active space self-consistent field (CASSCF) calculations. SIAZs studied in the present study are 2-silaazulene (2SIAZ) and 6-silaazulene (6SIAZ). The model reactions for the characterizations of 2SIAZ and 6SIAZ are an S_1–S_0 internal conversion (IC) process, which has been extensively studied on that of parent azulene. The initial processes of 2SIAZ and 6SIAZ upon electronic excitation into S_1 are similar to that of azulene, i.e. change from an aromatic geometry into a non-aromatic planar one. Contrary to the case of azulene, however, 2SIAZ and 6SIAZ in S_1 are further stabilized so as to take a non-planar geometry where the local geometry around the Si atom is non-planar. At the conical intersection between S_1 and S_0 (S_1/S_0-CIX) of 6SIAZ, only the seven-membered ring takes a non-planar geometry. On the other hand, both the five-membered and the seven-membered rings are non-planar at the S_1/S_0-CIX of 2SIAZ. Based on these computational findings, we characterize the SIAZ skeletons from a viewpoint of the excited state.

1. Introduction

Multiple bond compounds of heavier main group elements have been of great interest in the basic chemistry as well as the material science [1–3]. For the last several years, especially, this class of compounds has been intended to be utilized as photo-functional materials [4–7]. The idea of the applications to new photo-functional materials is based on the small HOMO–LUMO energy gap of multiple bond compounds, which makes it possible to tune the absorption and emission properties. In order to exploit excellent photo-functional molecules, however, the characterization of the excited states of multiple bond compounds is desirable. Recently we gave a new insight about the excited states of diphenyldiphosophene (PhP=PPh, Ph:phenyl group) which is an analogue of azobenzene (PhN=NPh) [8,9]. Though the electronic structures of diphenyldiphosphene are similar to those of azobenzene, the potential energy surfaces (PESs) in S_1 are very different from those of azobenzene. This implies that the photochemistry with the P=P compounds are different from that of the N=N compound of azobenzene. This could lead to a new photo-functional material with a P=P double bond. So we extend our interest to the photochemistry of heavier main group unsaturated bond compounds. In the present study, we focus our interest on 2-silaazulene (2SIAZ) and 6-silaazulene (6SIAZ) where the C^2 and C^6 atoms in the azulene skeleton are replaced by a Si atom, respectively. In the following paragraphs, we briefly mention why we chose silaazulenes (SIAZs) in the present study, although I will mention why 2SIAZ and 6SIAZ of six possible SIAZ isomers were chosen in the beginning of RESULTS section.

For the last decade, Tokitoh et al. have reported aromatic compounds containing Si atom such as silanaphthalenes [10–12] and silabenzenes [13] which are kinetically stabilized by bulky substituents. Computational approach gave a new insight of the bonding nature and reactivity of these aromatic compounds containing heavier group 14 elements [11,14–17]. On the other hand, there are no reports on non-benzenoid aromatic compounds containing Si atom. This is one reason why our present target is SIAZs.

Azulene is one of the most interesting molecules because of the unusual properties of the ground state as well as the excited states. Especially, the photochemical behavior, which violates Kasha's rule, has been extensively studied from experiment and theory since the first discovery in 1955 [18]. Recently we presented a new picture of the internal conversion (IC) of S_1–S_0 which allows us to interpret the recent experimental findings [19]. The most important point is that the conical intersection has no longer aromatic character but also take a non-planar geometry in the seven-membered ring. So our present concern is similarity and difference of the S_1–S_0 ICs of 2SIAZ, 6SIAZ and azulene. Thereby, we try to elucidate the intrinsic characters of the π conjugated silaazulene skeletons from a viewpoint of the S_1 state. This is another reason why we examine SIAZs to deepen understanding of multiple bond compounds.

The present paper is organized as follows. In the next section, we describe the method of calculation. In Section 3, we mention

* Tel.: +81 18 889 2625; fax: +81 18 889 2601.
E-mail address: amatatsu@ipc.akita-u.ac.jp.

1010-6030/$ – see front matter © 2010 Elsevier B.V. All rights reserved.
doi:10.1016/j.jphotochem.2010.05.023

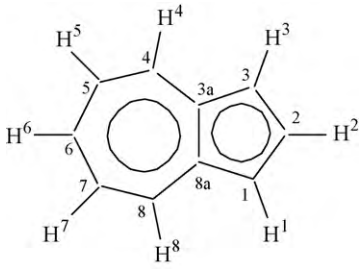

Fig. 1. Numbering of atoms and definition of the coordinates of the parent azulene. The *xy*-plane is spanned by an original molecular plane of S_0-geometry. The *z*-axis is perpendicular to the *xy*-plane.

the geometries and energies at important conformations of 2SIAZ and 6SIAZ. Then we analyze the reaction coordinates connecting important conformations with each other. Based on the computational findings, we discuss the photochemical behaviors of 2SIAZ and 6SIAZ in S_1, and characterize the π conjugated systems of SIAZs in comparison with that of azulene.

2. Method of calculation

First we performed configuration interaction (CI) calculations where up to triple excitations from the closed-shell configuration are taken into account. Thereby, we found that at most the highest five π occupied and the lowest five π* unoccupied orbitals are enough for the description of S_0 and S_1. So we adopted 10 electrons in 10 orbitals complete active space self-consistent field (denoted by (10,10)CASSCF) method, of which all the five π occupied and the lowest five π* unoccupied orbitals are included. Furthermore, we checked dynamic electron correlation effect on the stable geometry in S_0. As pointed out in the case of parent azulene [20–22], the dynamic electron correlation is essential to obtain a reasonable aromatic bond-equivalent structure in S_0 where the peripheral CC bonds are similar to an aromatic CC bond. As mentioned in Appendix A, the dynamic electron correlation effect is important at least in the case of the stable geometry in S_0 (S_0-geometry) of 6SIAZ, whereas it is much less important in the other cases (i.e. S_0-geometry of 2SIAZ, S_1-geometries of 2SIAZ and 6SIAZ). Therefore, we took the computational strategy same as in our previous calculations of azulene and 6-cyanoazulene [19,22]. We imposed the constraint of C_s symmetry (*xz*-plane in Fig. 1) to obtain a reasonable geometry of 6SIAZ in S_0, although in the other cases (i.e. 6SIAZ in S_1 and 2SIAZ in S_0 and S_1) the symmetry constraints are not always needed. In other words, planar geometries of 2SIAZ and 6SIAZ are designed to have C_{2v} symmetry but non-planar structures are also allowed under the constraint of C_s symmetry. However, we also emphasize that the discussion on the S_1–S_0 IC processes in S_1 is not affected by the above constraint, although that in S_0 after relaxation which is minor interest is affected in the case of 6SIAZ (see Appendix A in more detail). Therefore, the above constraint serves to save computational labor with little effect on the discussion of the S_1–S_0 IC processes, as pointed out in the cases of azulene and its derivative [22]. For the following reason, in addition, we did not perform second order multi-reference Møller–Plesset perturbation (MRMP2) calculations for energetic corrections. As pointed out previously [22], the shapes of the potential energy surfaces are not so changed by MRMP2 correction, although MRMP2 energies are lowered to be comparable to experimental values. This means that the CASSCF calculations are reliable enough to be proper for qualitative discussion. Our present purpose is characterizations of the SIAZ skeletons rather than comparison with experimental data.

First of all, we optimized four important conformations for the S_1–S_0 IC process of 2SIAZ; the minima in S_0 and S_1 (S_0-geometry and S_1-geometry), the stable planar geometry in S_1 (S_1-geometry(C_{2v})), and the conical intersection between S_1 and S_0 (S_1/S_0-CIX) where radiationless relaxation takes place. Only in the optimization of S_1/S_0-CIX, we adopted a smaller (8,8)CASSCF to reduce computational labor. After the determination of S_1/S_0-CIX by (8,8)CASSCF, however, we performed the present standard method of (10,10)CASSCF calculation at S_1/S_0-CIX to verify that the energy difference between S_1 and S_0 is small enough to be a CIX. This implies that a more terribly computationally demanding (10,10)CASSCF gives an S_1/S_0-CIX similar to that by (8,8)CASSCF. Next we calculated three types of the reaction paths (denoted by paths **A2**, **B2** and **C2**) which connect with the above four important geometries of 2SIAZ. Path **A2** starts from the S_0-geometry in S_1 and finally goes to the S_1-geometry passing through the S_1-geometry(C_{2v}). Path **B2** starts from the S_1/S_0-CIX to the S_1-geometry in S_1, while path **C2** goes to the globally stable S_0-geometry from the S_1/S_0-CIX in S_0.

We carried out similar calculations of 6SIAZ. That is, we optimized four important conformations of the S_1–S_0 IC process. Then we connected them with each other by means of the reaction paths. We will describe the more details in the relevant part.

Except for the determination of S_1/S_0-CIXs by Gaussian 03 [23], we used the GAMESS program with a basis set of Huzinaga–Dunning double-zeta and polarization functions (DZP) augmented on C ($\alpha_d = 0.75$) and Si ($\alpha_d = 0.395$) atoms [24].

Table 1
Standard bond distances containing a Si atom.[a]

Molecule	Bond	Bond distance
CH_3SiH_3	C–Si	1.887
C_5H_6Si (silabenzene)	CSi (aromatic)	1.762
$CH_2{=}SiH_2$	C=Si	1.697

[a] The values are optimized by MP2 with the same basis set of DZP in the present study.

3. Results

3.1. Geometrical features at important conformations

Before discussion on the geometrical features of 2SIAZ and 6SIAZ, we make two comments. One is what is meant by "aromaticity" in our present paper. Aromaticity has been conveniently used as a generic term to express the unique characters of π conjugated cyclic organic compounds such as benzene. However, there are various criteria about aromaticity, i.e. chemical reactivity, magnetic properties due to ring current, resonance energy, geometrical feature of bond length [25,26]. In our present paper, we use terms of "aromaticity" and/or "aromatic" from a viewpoint of the geometrical feature. That is, the bond distances of aromatic compounds are intermediate values between normal double bonds and single bonds (for instance, see Table 1 about SiC bonds). The other is why we chose 2SIAZ and 6SIAZ out of six possible SIAZ isomers. Preliminarily we examined the stable geometries of six possible SIAZs in S_0 by MP2 method. Thereby, we found that the most unstable species of 1SIAZ is non-aromatic and non-planar, whereas the others are planar and aromatic. 2SIAZ and 6SIAZ in S_0 are unstable only by 0.016 and 0.045 eV, respectively more than the most stable 4SIAZ. In addition, 2SIAZ and 6SIAZ are preferable to reduce computational labors of the full analyses of the reaction coordinates by virtue of the molecular symmetry. Of course, these symmetry constraints do not affect the results, as emphasized in the text some times.

Now we start to discuss the geometrical feature of the important conformations relevant to the S_1–S_0 IC process of 2SIAZ. Fig. 2 shows the optimized geometries of 2SIAZ with the skeletal bond distances, although the detailed geometrical parameters are listed in Table 2. Regarding the S_0-geometry, all the peripheral CC bond

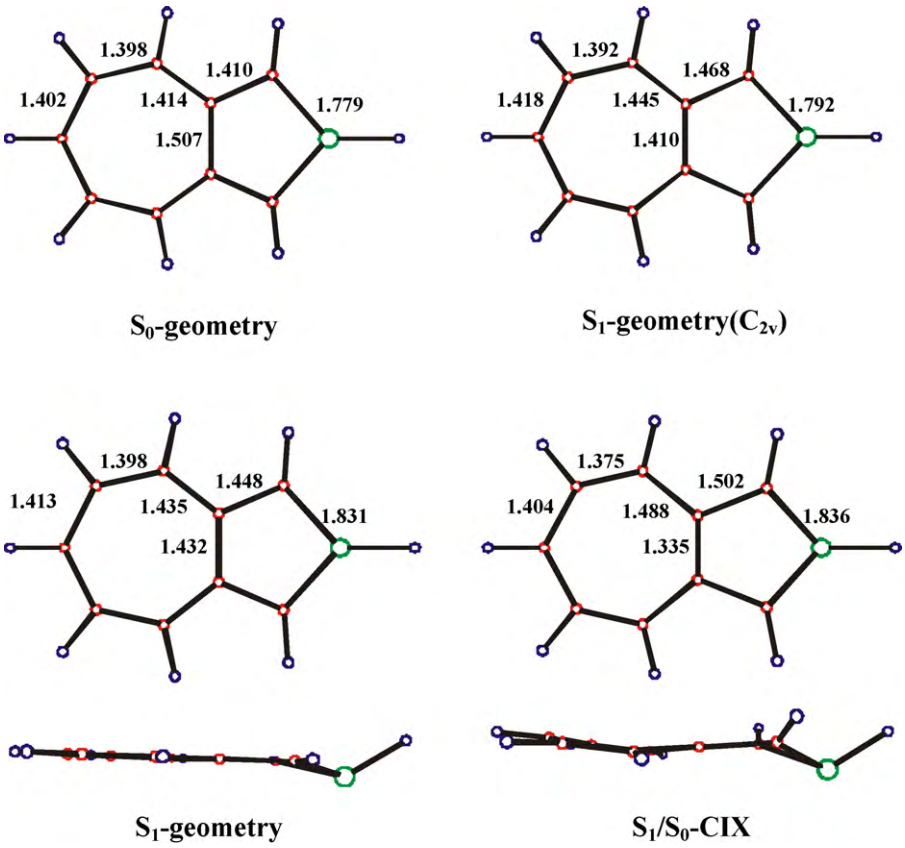

Fig. 2. Optimized geometries of 2SIAZ. The values are the optimized bond distances in Å. For more information on the geometries, the bond angles and the dihedral angles are given in Table 2. The lower panel of S_1-geometry and S_1/S_0-CIX is side views of respective geometries.

distances and the SiC (Si^2C^3 and Si^2C^1) ones are similar to aromatic CC and SiC bond distances, respectively. The transannular $C^{3a}C^{8a}$ bond is similar to a single CC bond. Considering that the S_0-geometry of 2SIAZ has C_{2v} symmetry, we can conclude that the S_0-geometry of 2SIAZ is also aromatic like that of parent azulene. The S_1-geometry(C_{2v}) which is the stable geometry with of C_{2v} symmetry in S_1 loses aromaticity in the 2SIAZ skeleton. That is, the transannular $C^{3a}C^{8a}$ bond shrinks and the bonds linked to the transannular bond (i.e. C^3C^{3a}, $C^{3a}C^4$, C^1C^{8a} and $C^{8a}C^8$) become longer. The change from S_0-geometry into S_1-geometry(C_{2v}) can be easily interpreted in terms of the HOMO (highest occupied molecular orbital) and LUMO (lowest unoccupied molecular orbital) (see Fig. 3) because the S_1 state is well described by the HOMO–LUMO single excitation as found in the case of azulene. For instance, the anti-bonding π^* character in the $C^{3a}C^{8a}$ part of the HOMO changes into the bonding π character of the LUMO so that the transannular $C^{3a}C^{8a}$ bond shrinks. So far the discussion resembles that of azulene [19]. Contrary to the case of azulene, however, 2SIAZ in S_1 is further stabilized by taking a non-planar structure in the five-membered ring (see the side view of S_1-geometry in Fig. 2 and also refer to the dihedral angles of $C^1Si^2C^3C^{3a}$ (−12.6°), $Si^2C^3C^{3a}C^{8a}$ (9.7°) and $H^2Si^2C^3C^{3a}$ (−136.3°) of S_1-geometry in Table 2). Relating to this non-planar geometry, it is found that the Si^2C^3 bond (1.831 Å) is longer than those at planar S_1-geometry(C_{2v}) (1.792 Å) and S_0-geometry (1.779 Å). The $C^1Si^2C^3$ (89.9°) and $H^2Si^2C^3$ (119.0°) angles are smaller than those at planar S_1-geometry(C_{2v}) (94.0° and 133.0°). The non-planarity of S_1-geometry is ascribed to the geometrical flexibility around the Si^2 atom in the 2SIAZ skeleton. The S_1/S_0-CIX also takes a non-planar geometry where the non-planarity in the five-membered ring becomes larger than that at the S_1-geometry and in addition the seven-membered ring is non-planar. Considering the relevant dihedral angles, it is found that the Si^2 and C^6 atoms are located opposite to the original molecular plane spanned by the S_0-geometry. This highly non-planar geometry of S_1/S_0-CIX is accessed from the S_1-geometry by additional changes: the transannular $C^{3a}C^{8a}$ bond further shrinks into a normal C=C double bond and the bonds linked to $C^{3a}C^{8a}$ becomes longer.

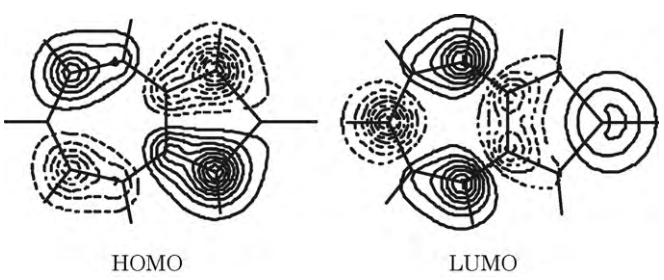

Fig. 3. HOMO and LUMO at the S_0-geometry of 2SIAZ.

In turn, we discuss the geometrical feature of the important conformations relevant to the S_1–S_0 IC process of 6SIAZ (see Fig. 4 and Table 2). The S_0-geometry of 6SIAZ is also planar and aromatic like that of 2SIAZ. The peripheral CC and SiC bonds are similar to aromatic CC and SiC bonds, respectively. The transannular $C^{3a}C^{8a}$ bond has single bond character. The S_1-geometry(C_{2v}) has geometrical feature similar to that of 2SIAZ; non-aromatic planar geometry. This change can be also understood in terms of the HOMO and LUMO in Fig. 5, considering that the S_1 state is also well described by the HOMO–LUMO single excitation. However, the change of the skeletal bond distances from the S_0-geometry into S_1-geometry(C_{2v}) is more drastic than that of 2SIAZ. The C^5Si^6 bond at S_1-geometry(C_{2v}) (1.823 Å) is much longer than the Si^2C^3 of 2SIAZ (1.792 Å), although

Table 2
Characteristic optimized parameters of 2SIAZ, 6SIAZ and azulene.[a]

	S_0-geometry			S_1-geometry(C_{2v})			S_1-geometry[b]			S_1/S_0-CIX		
Bond distances (Å)[c]												
2–3	1.779	1.406	1.410	1.792	1.400	1.405	1.831	1.400	–	1.836	1.384	1.401
3–3a	1.410	1.412	1.408	1.468	1.471	1.464	1.448	1.474	–	1.502	1.476	1.498
3a–4	1.414	1.406	1.396	1.445	1.461	1.445	1.435	1.459	–	1.488	1.459	1.487
4–5	1.398	1.402	1.404	1.392	1.373	1.387	1.398	1.365	–	1.375	1.366	1.332
5–6	1.402	1.776	1.404	1.418	1.823	1.424	1.413	1.854	–	1.404	1.857	1.461
3a–8a	1.507	1.504	1.498	1.410	1.394	1.390	1.432	1.389	–	1.335	1.387	1.359
Bond angles (°)[d]												
1–2–3	97.5	108.8	109.6	94.0	106.6	107.0	89.9	106.9	–	83.3	107.1	106.9
2–3–3a	106.8	109.6	108.6	108.7	109.9	109.2	110.5	109.6	–	111.7	110.0	109.2
3–3a–8a	114.5	106.1	106.6	114.3	106.8	107.3	113.5	107.0	–	111.6	106.5	107.3
4–3a–8a	125.6	132.4	127.7	127.5	134.2	129.4	127.1	133.1	–	128.5	133.3	128.8
5–4–3a	131.3	131.2	128.6	129.4	129.6	126.8	129.8	129.4	–	126.1	129.1	125.3
6–5–4	129.1	125.9	128.8	129.6	126.8	129.5	129.5	127.6	–	130.6	127.5	128.7
7–6–5	127.9	120.9	129.7	127.1	118.7	128.6	127.1	111.8	–	127.1	111.9	125.4
H–Si–C	131.3	119.6	–	133.0	120.6	–	119.0	110.9	–	113.7	110.7	–
Dihedral angles (°)[e]												
1–2–3–3a	0.0	0.0	0.0	0.0	0.0	0.0	−12.6	0.6	–	−27.7	0.5	−0.6
2–3–3a–8a	0.0	0.0	0.0	0.0	0.0	0.0	9.7	−0.3	–	22.0	−0.3	0.4
5–4–3a–8a	0.0	0.0	0.0	0.0	0.0	0.0	0.9	14.1	–	14.3	14.0	19.4
6–5–4–3a	0.0	0.0	0.0	0.0	0.0	0.0	−0.6	5.3	–	−8.8	5.4	−3.2
7–6–5–4	0.0	0.0	0.0	0.0	0.0	0.0	−0.2	−28.4	–	−5.8	−28.5	−26.6
H–Si–C–C	180.0	180.0	180.0	180.0	180.0	180.0	−136.3	−152.7	–	−140.7	−152.6	–

[a] Each cell composes of triplet values in a row. The first, the second and the third values are optimized parameters of 2SIAZ, 6SIAZ and azulene, respectively. The values of azulene are taken from Ref. [19].

[b] The third values of S_1-geometry are in blank because the most stable geometry in S_1 of azulene takes a C_{2v} geometry. So the S_1-geometry(C_{2v}) is same as the S_1-geometry of azulene.

[c] The bond distances are indicated by doublet numbers. For instance, 2–3 of 2SIAZ means the bond distances of Si^2C^3. Due to symmetry constraint of C_s, the Si^2C^1 bond of 2SIAZ is equivalent to the Si^2C^3 bond.

[d] The bond angles are indicated by triplet numbers or letters. For instance, 2–3–3a and H–Si–C of 2SIAZ mean the bond angles of $Si^2C^3C^{3a}$ and $H^2Si^2C^3$, respectively. Due to symmetry constraint of C_s, $Si^2C^1C^{8a}$ and $H^2Si^2C^1$ are equivalent to $Si^2C^3C^{3a}$ and $H^2Si^2C^3$. In the case of 6SIAZ, H–Si–C means $H^6Si^6C^5$.

[e] The dihedral angles are indicated by quartet numbers or letters. For instance, 1–2–3–3a and H–Si–C–C of 2SIAZ mean the dihedral angles of $C^1Si^2C^3C^{3a}$ and $H^2Si^2C^3C^{3a}$, respectively. Due to symmetry constraint of C_s, $C^3Si^2C^1C^{8a}$ and $H^2Si^2C^1C^{8a}$ are the values of $C^1Si^2C^3C^{3a}$ and $H^2Si^2C^3C^{3a}$ with opposite signs, respectively.

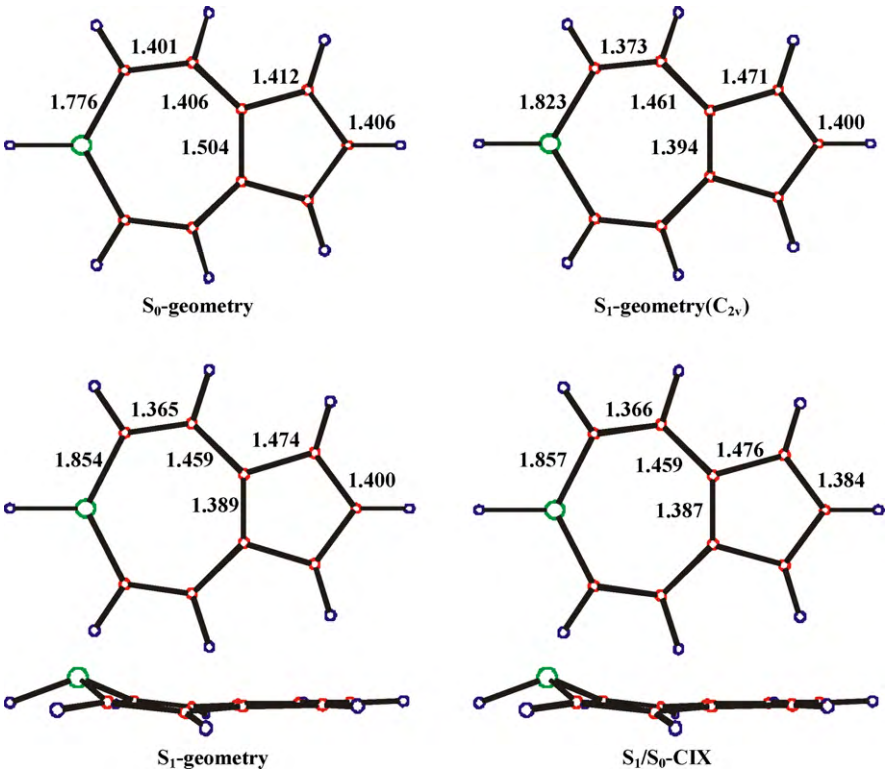

Fig. 4. Optimized geometries of 6SIAZ. The values are the optimized bond distances in Å. For more information on the geometries, the bond angles and the dihedral angles are given in Table 2. The lower panel of S_1-geometry and S_1/S_0-CIX is side views of respective geometries.

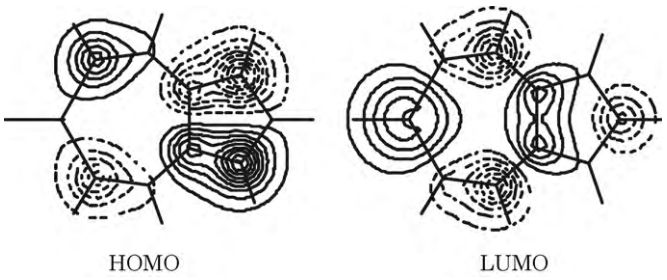

Fig. 5. HOMO and LUMO at the S_0-geometry of 6SIAZ.

both of them at S_0-geometries are similar to an aromatic SiC bond distance. The changes of the CC bonds in the seven-membered ring are larger than those of 2SIAZ. The most stable geometry in S_1 (S_1-geometry) of 6SIAZ takes a non-planar geometry in the seven-membered ring (see the dihedral angles of $C^5C^4C^{3a}C^{8a}$ (14.1°), $Si^6C^5C^4C^{3a}$ (5.3°), $C^7Si^6C^5C^4$ (−28.4°) and $H^6Si^6C^5C^4$ (−152.6°) in the relevant part of Table 2), while the five-membered ring is planar. This non-planarity of the S_1-geometry can be rationalized by a principle similar to that of 2SIAZ; the geometrical flexibility around the Si^6 atom at S_1-geometry. Contrary to the case of 2SIAZ, however, the skeletal bond distances almost remains unchanged except for the C^5Si^6 bond. In a further C^5Si^6 elongation of the S_1-geometry(C_{2v}) to S_1-geometry (1.823–1.854 Å), only the geometry around the Si^6 atom is affected; the bond angles of $C^5Si^6C^7$ (118.7–111.8°) and $H^6Si^6C^5$ (120.6–110.9°) become smaller and the dihedral angles of $H^6Si^6C^5C^4$ (−152.6°) and $C^7Si^6C^5C^4$ (−28.4°) deviate from those at the planar geometry (180° and 0°, respectively). In other words, most of the 6SIAZ skeleton is already relaxed at planar S_1-geometry(C_{2v}) and so additional change of the non-planarity affects only the local geometry around the Si^6 atom. The S_1/S_0-CIX of 6SIAZ is very similar to the S_1-geometry. This implies that the S_1/S_0-CIX is located around the S_1-geometry. We will make additional comment from a viewpoint of energy in the following subsection.

3.2. Energetics

Table 3 lists the energies at important conformations for 2SIAZ and 6SIAZ as well as parent azulene by the present standard method of (10,10)CASSCF. First of all we mention the validity of S_1/S_0-CIXs by (8,8)CASSCF. At S_1/S_0-CIXs, the energy differences between S_0 and S_1 (0.092 eV for 2SIAZ, 0.019 eV for 6SIAZ) are small even by (10,10)CASSCF. This implies that a much more computational demanding (10,10)CASSCF gives S_1/S_0-CIXs similar to those by (8,8)CASSCF.

Table 3
Energies (eV) at important conformations of 2SIAZ, 6SIAZ and azulene.

	S_0-geometry	S_1-geometry(C_{2v})	S_1-geometry (C_s)	S_1/S_0-CIX[a]
2SIAZ				
S_0	0.0	0.387	0.392	2.414
S_1	2.173	1.896	1.576	2.322
6SIAZ				
S_0	0.0	0.567	0.899	0.971
S_1	1.827	1.390	0.975	0.990
Azulene[b]				
S_0	0.0	0.500		1.803
S_1	1.952	1.556		1.981

[a] The energies in S_0 and S_1 at S_1/S_0-CIX are not exactly same. This is because S_1/S_0-CIX geometry is optimized by (8,8)CASSCF but the energies are evaluated by the present standard (10,10)CASSCF. Of course, the energies by (8,8)CASSCF are same.
[b] The values are taken from Ref. [19].

As deduced from the above discussion on the geometrical features of 2SIAZ, the energy of 2SIAZ in S_1 is lowered according to the geometrical changes of S_0-geometry → S_1-geometry(C_{2v}) → S_1-geometry. However, the S_1/S_0-CIX is energetically unstable more than the S_1-geometry, which is similar to the case of azulene [19]. Regarding 6SIAZ, the energetics of the S_0-geometry to the S_1-geometry is similar to that of 2SIAZ. Contrary to the case of 2SIAZ, however, the S_1/S_0-CIX is almost same as S_1-geometry and the energy difference between S_1 and S_0 is only 0.076 eV even at the S_1-geometry. This implies that the S_1/S_0-CIX of 6SIAZ is located in the vicinity of the S_1-geometry.

3.3. Reaction coordinates of S_1–S_0 IC processes

Reaction coordinate analysis is a powerful tool to obtain insight about internal mode couplings of chemical process on the multi-dimensional potential energy surfaces. In this subsection, we try to connect the above important geometries with each other by intrinsic reaction coordinates to discuss the S_1–S_0 IC processes of 2SIAZ and 6SIAZ in detail. Fig. 6 shows the energy profiles of 2SIAZ along paths **A2**, **B2** and **C2**. Path **A2**, for which the reaction coordinate is labeled as s_{A2} in bohr amu$^{1/2}$, starts from S_0-geometry in S_1 and goes to the most stable geometry in S_1 (i.e. S_1-geometry) (see Fig. 6a). Paths **B2** and **C2**, for which the reaction coordinate is labeled as s_{BC2} (in bohr amu$^{1/2}$) in Fig. 6b, start from the S_1/S_0-CIX and go respectively to S_1-geometry in S_1 and S_0-geometry in S_0. From the energy profiles, the S_1–S_0 IC of 2SIAZ consists of three processes; paths **A2**, **B2** and **C2**. In path **A2** after electronic excitation into S_1, it is found that electronically excited 2SIAZ is stabilized by two steps; $0 \le s_{A2} \le 1.133$ and $s_{A2} \ge 1.133$, where $s_{A2} = 1.133$ corresponds to the S_1-geometry(C_{2v}) at an inflection point in Fig. 6a. In the first step (i.e. $0 \le s_{A2} \le 1.133$) 2SIAZ remains planar, while the bond distances change greatly (the details of the geometrical changes along the reaction coordinates are provided in the Supplementary data). The transannular $C^{3a}C^{8a}$ bond quickly shrinks and concomitantly the bonds linking to the $C^{3a}C^{8a}$ bond (i.e. C^3C^{3a}, $C^{3a}C^4$,C^1C^{8a} and $C^{8a}C^8$) become longer. This skeletal change can be understood in terms of the HOMO and LUMO (refer to Fig. 3), as mentioned in 3-1. In the second step of S_1-geometry(C_{2v}) → S_1-geometry (i.e. $s_{A2} \ge 1.133$), 2SIAZ becomes non-planar in the five-membered ring. In this step, the angles of $C^1Si^2C^3$ and $H^2Si^2C^3$ decrease and interestingly only the Si^2C^3 (and Si^2C^1) bond of the skeletal bonds becomes longer. This means that the local geometry around the Si atom changes from a planar trigonal geometry to a non-planar pyramidal one in $s_{A2} \ge 1.133$. In other words, the second step is ascribed to a change of the hybridization from sp^2 into sp^3 on the Si^2 atom. On the basis of the above discussion, path **A2** can be regarded as follow. First the skeletal relaxation of 2SIAZ in S_1 takes place with a planar geometry. This event destroys the aromaticity and weakens the 2SIAZ skeleton, which allows 2SIAZ to cause further relaxation of a non-planar geometry in the five-membered ring containing a Si atom.

Path **B2** of S_1-geometry → S_1/S_0-CIX in S_1 (i.e $s_{BC2} \le 0.0$ in Fig. 6b) is energetically uphill to reach the S_1/S_0-CIX at $s_{BC2} = 0.0$ in S_1. In this process, the five-membered ring enhances its non-planarity but also the seven-membered ring becomes non-planar (refer to Table 2 and the Supplementary data). The transannular $C^{3a}C^{8a}$ bond and the bonds linking to $C^{3a}C^{8a}$ change greatly, especially in the vicinity of S_1/S_0-CIX. The $C^{3a}C^{8a}$ bond shrinks into a C=C double bond, while the bonds linking to $C^{3a}C^{8a}$ elongate to a C–C single bond. The features of the energy profile and geometrical changes in the seven-membered ring in path **B2** are similar to those of azulene [19].

In path **C2** of S_1/S_0-CIX → S_0-geometry in S_0 (i.e $s_{BC2} \ge 0.0$ in Fig. 6b), the reaction coordinate is followed in S_0. The transannular $C^{3a}C^{8a}$ bond quickly elongates up to a normal C–C single bond

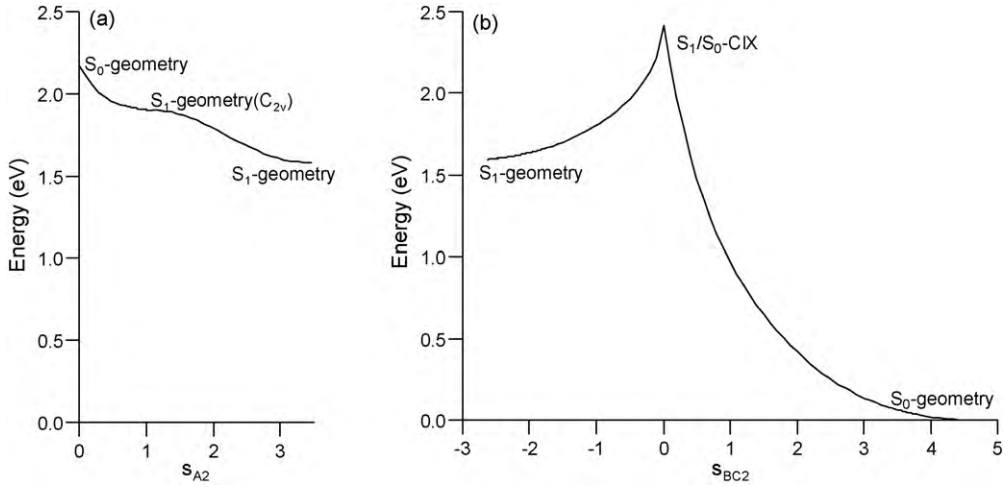

Fig. 6. Potential energy profiles along the reaction coordinates in bohr amu$^{1/2}$ of 2SIAZ: (a) path **A2**, (b) paths **B2** ($s_{BC2} \leq 0.0$) and **C2** ($s_{BC2} \geq 0.0$).

and all the peripheral CC bonds quickly converge to an aromatic CC bond distance (see the the Supplementary data about the details). In other words, the skeletal recovery of aromatic S_0-geometry except for the SiC bonds is completed during the early stage after relaxation into S_0 (i.e. $0.0 \leq s_{BC2} \leq 1.8$). Contrary to the quick change of the CC bond distances, the SiC bond distances, the bond angles and dihedral angles gradually recover to those at planar aromatic S_0-geometry. This implies that the SiC stretchings are softer than the CC stretchings and the skeletal in-plane and out-of-plane deformations are more floppy even in S_0.

In turn we discuss the S_1–S_0 IC of 6SIAZ in comparison with that of 2SIAZ mentioned above. Fig. 7 shows the energy profiles of 6SIAZ along the paths **A6** and **C6**. Paths **A6** and **C6** connect from the S_0-geometry in S_1 to the S_1-geometry, and from the S_1/S_0-CIX to the S_0-geometry in S_0, respectively. However, path **B6**, which corresponds to path **B2** connecting the S_1-geometry with the S_1/S_0-CIX of 2SIAZ in S_1, is missing. As mentioned in the previous subsection, the S_1/S_0-CIX of 6SIAZ is very similar to the S_1-geometry. Actually, we followed the reaction path from the S_1/S_0-CIX to the S_1-geometry in S_1. The distance of the reaction path is only 0.16 bohr amu$^{1/2}$ and the energy is lowered only by 0.013 eV on this path. So the S_1-geometry can be substantially regarded as the S_1/S_0-CIX and it is proper that the S_1–S_0 IC of 6SIAZ is path **A6** → path **C6**, contrary to the case of path **A2** → path **B2** → path **C2** of 2SIAZ.

The first process of path **A6** consists of two steps, as same in the case of path **A2** of 2SIAZ. Up to the inflection point at $s_{A6} = 1.078$ of S_1-geometry(C_{2v}) (i.e. $0 \leq s_{A6} \leq 1.078$ in Fig. 7a), the skeletal relaxation takes place with a C_{2v} planar geometry (the details of the geometrical changes along the reaction coordinates are provided in the the Supplementary data). In concomitant with the shortening of the transannular $C^{3a}C^{8a}$ in $0 \leq s_{A6} \leq 1.078$ (i.e. S_0-geometry → S_1-geometry(C_{2v}) in S_1), the bonds linking to the $C^{3a}C^{8a}$ bond become longer. These changes are similar to those of 2SIAZ. However, the C^4C^5 and C^5Si^6 (also C^8C^7 and C^7Si^6) bonds also change greatly, while the C^4C^5 and C^5C^6 bonds of 2SIAZ little change in the first step. The C^4C^5 bond of 6SIAZ shrinks quickly and the C^5Si^6 elongates. In other words, the loss of the aromaticity is more apparent than that of 2SIAZ in the first step of path **A2**. This can be rationalized by the following two factors. One factor is that an aromatic SiC π bond is more fragile than an aromatic CC π bond so that the SiC bond can easily elongate through electronic excitation into S_1. This factor is common to 6SIAZ and 2SIAZ, but the following factor is more favorable for 6SIAZ. A seven-membered ring has more internal degrees of freedom with respect to the skeletal stretchings more than a five-membered ring. So at a planar conformation of 6SIAZ, a seven-membered ring is more favorable to skeletally relax in S_1 only by changing the skeletal bond distances. Therefore, in the first step (i.e. aromatic S_0-geometry to non-aromatic S_1-geometry(C_{2v})), 6SIAZ can skeletally relax more than 2SIAZ. In the second step of S_1-geometry(C_{2v}) → S_1-geometry, the seven-membered ring comes to take a non-planar geometry so that 6SIAZ in S_1 becomes more stable. This is different from the case that the five-membered ring of 2SIAZ comes to takes a non-planar geometry. In either case, however, a ring where the C atom in the azulene skeleton is replaced by a Si atom is non-planar. On the other hand, the stable azulene in S_1 is planar. This can be easily understood by the former factor mentioned above. Due to a fragile SiC π bond, a SIAZ skeleton in S_1 becomes more flexible with respect to the out-of-plane motion of the ring where the C atom is replaced by a Si atom. In consequence, the S_1-geometries of 6SIAZ and 2SIAZ are non-planar. On the other hand, azulene which does not include a Si atom in the skeleton has no additional flexibility of a non-planarity to be more stable.

Path **C6** of S_1/S_0-CIX → S_0-geometry in S_0 (i.e. $0.0 \leq s_{C6}$) corresponds to a relaxation process in S_0 after the transition from S_1 into S_0 at the S_1/S_0-CIX. The aromatic 6SIAZ skeleton is recovered quickly except for the CSi bonds. On the other hand, the stretched CSi bonds, the in-plane and the out-of-plane deformations are recovered gradually. This is similar to the case of path **C2** of 2SIAZ.

3.4. Characterization of π conjugated systems of 2SIAZ and 6SIAZ

Based on the above discussions, we characterize the π conjugated systems of 2SIAZ and 6SIAZ. First we review the IC of azulene briefly, though we previously reported it in detail [19]. The aromatic S_0-geometry in S_1 skeletally relaxes into a non-aromatic planar S_1-geometry(C_{2v}) which is a globally stable geometry in S_1. Due to the loss of aromaticity around the S_1-geometry(C_{2v}), the S_1-geometry(C_{2v}) of azulene becomes more flexible with respect to the out-of-plane motion in the seven-membered ring so as to reach the non-planar S_1/S_0-CIX along the uphill potential energy surface in S_1. In the process of S_1-geometry(C_{2v}) → S_1/S_0-CIX in S_1, the out-of-plane motion is promoted. This is the origin of the strong oscillation assignable to the out-of-plane motion by the femtosecond time-resolved spectroscopic experiment [27].

Regarding the S_1–S_0 IC of 2SIAZ (see Fig. 6), the aromatic S_0-geometry in S_1 skeletally relaxes into the non-aromatic planar S_1-geometry(C_{2v}) and becomes further stable into the non-planar S_1-geometry where only the five-membered ring is non-planar. To access the S_1/S_0-CIX from the S_1-geometry, 2SIAZ is destabilized by non-planarity in the seven-membered ring as well as enhance-

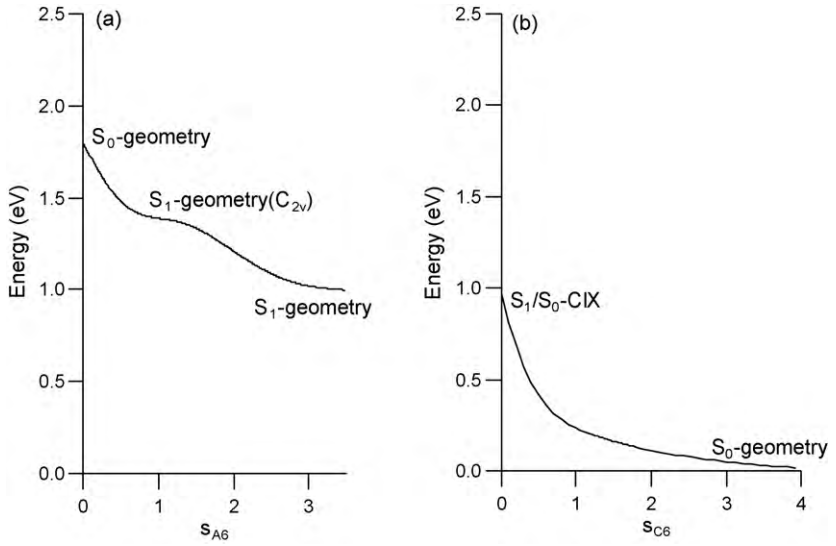

Fig. 7. Potential energy profiles along the reaction coordinates in bohr amu$^{1/2}$ of 6SIAZ: (a) path **A6** and (b) path **C6**. As mentioned in the text, S_1-geometry is substantially same as S_1/S_0-CIX.

ment of the non-planarity in the five-membered ring. In the process of S_1-geometry(C_{2v}) → S_1-geometry → S_1/S_0-CIX, the out-of-plane motions are promoted like the case of azulene. Once relaxation into S_0 takes place at the S_1/S_0-CIX, the non-planar S_1/S_0-CIX quickly changes into the aromatic planar S_0-geometry.

From the shape of the energy profile of 6SIAZ in Fig. 7, it can be deduced that the S_1–S_0 IC of 6SIAZ is different from those of 2SIAZ and azulene. The process of S_0-geometry → S_1-geometry(C_{2v}) → S_1-geometry in S_1 is similar to that of 2SIAZ. However, the S_1/S_0-CIX of 6SIAZ is substantially same as S_1-geometry. So 6SIAZ around the S_1-geometry immediately relaxes into S_0, contrary to the cases that the S_1-geometries of 2SIAZ and azulene change into the S_1/S_0-CIXs on the uphill potential energy surfaces and then relax into S_0. This implies that the S_1–S_0 IC process of 6SIAZ is much faster than those of 2SIAZ and azulene so that the out-of-plane motion of 6SIAZ is promoted only during much shorter period. In order to make these differences of the dynamics clear, a molecular dynamics simulation is desirable.

For the present, the dynamics of the S_1–S_0 IC processes mentioned above is speculative because there are no reports on the syntheses of 2SIAZ and 6SIAZ including their derivatives protected by bulky substituents. However, the above discussion is worthwhile to characterize the π conjugated systems of 2SIAZ and 6SIAZ skeleton as well as that of azulene. From Figs. 6 and 7, the potential energy surfaces relating to the S_1–S_0 IC processes of SIAZs are highly dependent on the replacement position of a Si atom in the azulene skeleton. In all the cases of 2SIAZ, 6SIAZ and azulene, the aromatic bond-equivalent skeletons in the peripheral bonds are easily destroyed by electronic excitation into S_1 and turn to be non-aromatic. In the case of azulene, the non-aromatic planar structure (S_1-geometry(C_{2v})) is stable in S_1 but the energy difference between S_1 and S_0 is large (1.056 eV from the relevant part in Table 3). However, the out-of-plane motion in the seven-membered ring is soft in S_1, whereas it is very hard in S_0. This causes an energetic closeness of S_1 and S_0 around the S_1-geometry. This is a qualitative explanation to why S_1/S_0-CIX is located around the non-aromatic S_1-geometry with a non-planar geometry in the seven-membered ring. The replacement by a Si atom in the azulene skeleton makes the out-of-plane motion more flexible in S_1. In the case of 2SIAZ, the non-aromatic S_1-geometry(C_{2v}) becomes more stable into the non-planar S_1-geometry where the Si[2] atom in the five-membered ring is located out of the plane of S_1-geometry(C_{2v}). Even in the case of 2SIAZ, however, the seven-membered ring is planar around the S_1-geometry and the energy difference between S_1 and S_0 is large (1.184 eV from the relevant part in Table 3), which is same as the case of azulene. Therefore, the non-planarity in the seven-membered ring is essential to an energetic closeness of S_1 and S_0 even in the case of 2SIAZ. In the case of 6SIAZ, we can easily understand why the S_1-geometry takes a non-planar geometry in the seven-membered ring by the same principle mentioned above. Considering another factor that a non-planarity of the seven-membered ring is very important for the energetic closeness of S_1 and S_0, the S_1-geometry of 6SIAZ already has this factor and little additional changes from the S_1-geometry into the S_1/S_0-CIX are needed. This is a qualitative explanation to why the S_1/S_0-CIX of 6SIAZ is located in the vicinity of the S_1-geometry.

4. Concluding remarks

In this paper, we characterized SIAZ skeletons by the reaction coordinates of S_1–S_0 ICs of 2SIAZ and 6SIAZ. The early stages of these processes are similar to that of azulene. Upon electronic excitation into S_1, the bond-equivalent aromatic geometries in S_0 change into the non-aromatic ones with C_{2v} symmetry. However, the non-aromatic planar geometries of 2SIAZ and 6SIAZ in S_1 are further stabilized by taking a non-planar geometry where the local geometry around the Si atom is non-planar. The S_1/S_0-CIX of 6SIAZ is similar to that of azulene where only the seven-membered ring takes a non-planar geometry. On the other hand, the S_1/S_0-CIX of 2SIAZ takes a non-planar geometry where both the five-membered and the seven-membered rings are non-planar. Contrary to the geometrical similarity at the S_1/S_0-CIXs of 6SIAZ and azulene, the shapes of the potential energy surfaces around the S_1/S_0-CIX are very different from those of azulene. The S_1/S_0-CIX of 6SIAZ is, in a sense, classified as a peaked type, whereas those of azulene as well as 2SIAZ are a sloped type [28]. These features can be qualitatively explained by the following principles, of which the first three are common to SIAZs as well as azulene:

(P1) the azulene, 2SIAZ and 6SIAZ skeletons easily lose their aromaticity upon electronic excitation into S_1.
(P2) these skeletons in S_1 become more flexible with respect to the out-of-plane motion in S_1.
(P3) the potential energy in S_0 with respect to the out-of-plane mode in the seven-membered ring increases much more than that in S_1.

Table A.1
Dependency of the stable geometries of 2SIAZ and 6SIAZ in S_0 on computational method.

Method	RHF	(10,10)CASSCF	(10,10)CASSCF/C_{2v}[a]	MP2
2SIAZ				
Si^2C^3(Si^2C^1)	1.760(1.760)[b]	1.778(1.781)	1.779	1.777(1.777)
C^3C^{3a}(C^1C^{8a})	1.406(1.406)	1.411(1.408)	1.410	1.417(1.416)
$C^{3a}C^4$($C^{8a}C^8$)	1.404(1.404)	1.412(1.415)	1.414	1.415(1.415)
C^4C^5(C^8C^7)	1.387(1.387)	1.400(1.397)	1.398	1.403(1.403)
C^5C^6(C^7C^6)	1.390(1.390)	1.401(1.404)	1.402	1.406(1.406)
$C^{3a}C^{8a}$	1.501	1.507	1.507	1.505
6SIAZ				
C^2C^3(C^2C^1)	1.396(1.395)	1.376(1.440)	1.406	1.409(1.409)
C^3C^{3a}(C^1C^{8a})	1.404(1.404)	1.445(1.386)	1.412	1.420(1.420)
$C^{3a}C^4$($C^{8a}C^8$)	1.405(1.404)	1.381(1.437)	1.406	1.407(1.407)
C^4C^5(C^8C^7)	1.389(1.389)	1.431(1.377)	1.401	1.403(1.403)
C^5Si^6(C^7Si^6)	1.762(1.761)	1.749(1.807)	1.776	1.773(1.773)
$C^{3a}C^{8a}$	1.480	1.501	1.504	1.501

[a] The geometries are optimized under constraint of C_{2v} symmetry.
[b] The numbers in the parentheses are the corresponding bond distances in Fig. 1.

(P4) replacement by a Si atom in azulene skeleton weakens the aromaticity of SIAZ skeleton. Thereby, the out-of-plane motion concerning the Si atom is promoted in S_1 more than that of parent azulene.

Finally, we make comment on a perspective of the silaazulene chemistry. As reviewed in Section 1, silabenzene and silanaphthalene have proven to hold aromatic geometrical character experimentally and theoretically. On the other hand, there is no report about non-benzenoid aromatic compounds of heavier main group elements such as silaazulene. In the present study, we found that the silaazulene aromatic skeleton of 2SIAZ and 6SIAZ are more fragile than that of parent azulene, which leads to a photochemical behavior different from that's of azulene. However, the present model molecules of bare 2SIAZ and 6SIAZ might be too simple for a realistic silaazulene to be examined, although the characters of the silaazulene skeletons are expected to be hold with/without a bulky substituent. So our next concern is whether a realistic silaazulene protected by bulky substituent holds aromaticity in S_0. We are now in progress on the study of a geometry of realistic silaazulene with a bulky substituent in S_0 to promote a synthetic work on silaazulenes or more generally non-benzenoid Si-containing aromatic compounds.

Acknowledgments

This work is financially supported by Grant-in-Aid for Priority Area (Molecular Theory for Real Systems) (Nos. 19029004 and 20038004) from the Ministry of Education, Culture, Sports, Science and Technology.

Appendix A.

In the case of azulene, as pointed out previously [19–22], the stable geometry in S_0 is highly dependent on computational method. Restricted Hartree–Fock (RHF) and CASSCF calculations where at most static electron correlation are taken into account give a unreasonable bond-alternant geometry where a C=C double and a C–C single bond of the peripheral bonds alternate with each other. On the other hand, calculations where the dynamic electron correlation effect is also included (for instance, the second order Møller–Plesset perturbation (MP2) method) give a reasonable bond-equivalent geometry where all the peripheral CC bonds are similar to an aromatic CC bond. So we checked if the stable geometries in S_0 of 2SIAZ and 6SIAZ depend on the computational method. As seen from Table A.1, the methods tested here (i.e. RHF, CASSCF and MP2) give reasonable bond-equivalent geometries in S_0 except for the S_0-geometry of 6SIAZ by (10,10)CASSCF. Even in this case, the S_0-geometry by (10,10)CASSCF is energetically more unstable by 0.014 eV than that by (10,10)CASSCF under C_{2v} constraint. In conclusion, dynamic electron correlation is much less important to obtain reasonable S_0-geometries of 2SIAZ and 6SIAZ, contrary to the case of azulene. In the case of 6SIAZ, however (10,10)CASSCF without proper symmetry constraint leads to a wrong discussion. Therefore, we took the computational strategy same as in the case of azulene. That is, we imposed the constraint of C_s symmetry (the *xz*-plane is the symmetry plane in Fig. 1) which allows 2SIAZ and 6SIAZs to take a reasonable planar bond-equivalent geometry in S_0 and furthermore to take a non-planar geometry around the S_1/S_0-CIXs.

Concerning the stable geometries in S_1, on the other hand (10,10)CASSCF calculations without any symmetry constraint give the same results under the above constraint. This means that the shapes of the potential energy surfaces in S_1 are little affected by the above constraint. Therefore, the S_1–S_0 IC processes of 2SIAZ and 6SIAZ in S_1, which is main interest in the present study, are not affected by the symmetry constraint. On the other hand, in the IC process after relaxation into S_0 which is minor interest in the present study, the symmetry constraint is important so as to avoid relaxing into a wrong bond-alternant geometry in S_0, especially in the case of 6SIAZ. In conclusion, the symmetry constraint in the present calculations serves to reduce the computational labor, while it gives the same result without any symmetry constraint, as previously pointed out in the case of azulene and its derivatives [22].

Appendix B. Supplementary data

Supplementary data associated with this article can be found, in the online version, at doi:10.1016/j.jphotochem.2010.05.023.

References

[1] L. Weber, Chem. Rev. 92 (1992) 1839–1906.
[2] P.P. Power, Chem. Rev. 99 (1999) 3463–3503.
[3] F. Mathey, Angew. Chem. Int. Ed. 42 (2003) 1578–1603.
[4] V.A. Wright, D.P. Gates, Angew. Chem. Int. Ed. 41 (2002) 2389–2392.
[5] R.C. Smith, J.D. Protasiewicz, J. Am. Chem. Soc. 126 (2004) 2268–2269.
[6] S. Kawasaki, A. Nakamura, K. Toyota, M. Yoshifuji, Bull. Chem. Soc. Jpn. 78 (2005) 1110–1120.
[7] T. Baumgartner, R. Réau, Chem. Rev. 106 (2006) 4681–4727.
[8] Y. Amatatsu, J. Phys. Chem. A 112 (2008) 8824–8828.
[9] Y. Amatatsu, J. Phys. Chem. A 113 (2009) 9667–9674.
[10] N. Tokitoh, K. Wakita, R. Okazaki, S. Nagase, P.v.R. Schleyer, H. Jiao, J. Am. Chem. Soc. 119 (1997) 6951–6952.
[11] K. Wakita, N. Tokitoh, R. Okazaki, S. Nagase, P.v.R. Schleyer, H. Jiao, J. Am. Chem. Soc. 121 (1999) 11336–11344.

[12] A. Shinohara, N. Takeda, T. Sasamori, N. Tokitoh, Bull. Chem. Soc. Jpn. 78 (2005) 977–987.
[13] K. Wakita, N. Tokitoh, R. Okazaki, N. Takagi, S. Nagase, J. Am. Chem. Soc. 122 (2000) 5648–5649.
[14] K.K. Baldridge, O. Uzan, J.M.L. Martin, Organometallics 19 (2000) 1477–1487.
[15] U.D. Priyakumar, G.N. Sastry, Organometallics 21 (2002) 1493–1499.
[16] A.M. El-Nahas, M. Johansson, H. Ottosson, Organometallics 22 (2003) 5556–5566.
[17] N. Tokitoh, Bull. Chem. Soc. Jpn. 77 (2004) 429–441.
[18] M. Beer, H.C. Longuet-Higgins, J. Chem. Phys. 23 (1955) 1390–1391.
[19] Y. Amatatsu, Y. Komura, J. Chem. Phys. 125 (2006) 174311/1–174311/8 (The review on the azulene photochemistry is therein).
[20] P.M. Kozlowski, G. Rauhut, P. Pulay, J. Chem. Phys. 103 (1995) 5650–5661.
[21] A. Murakami, T. Kobayashi, A. Goldberg, S. Nakamura, J. Chem. Phys. 120 (2004) 1245–1252.
[22] Y. Amatatsu, J. Phys. Chem. A 111 (2007) 5327–5332.
[23] M.J. Frisch, G.W. Trucks, H.B. Schlegel, G.E. Scuseria, M.A. Robb, J.R. Cheeseman, J.A. Montgomery Jr., T. Vreven, K.N. Kudin, J.C. Burant, J.M. Millam, S.S. Iyengar, J. Tomasi, V. Barone, B. Mennucci, M. Cossi, G. Scalmani, N. Rega, G.A. Petersson, H. Nakatsuji, M. Hada, M. Ehara, K. Toyota, R. Fukuda, J. Hasegawa, M. Ishida, T. Nakajima, Y. Honda, O. Kitao, H. Nakai, M. Klene, X. Li, J.E. Knox, H.P. Hratchian, J.B. Cross, C. Adamo, J. Jaramillo, R. Gomperts, R.E. Stratmann, O. Yazyev, A.J. Austin, R. Cammi, C. Pomelli, J.W. Ochterski, P.Y. Ayala, K. Morokuma, G.A. Voth, P. Salvador, J.J. Dannenberg, V.G. Zakrzewski, S. Dapprich, A.D. Daniels, M.C. Strain, O. Farkas, D.K. Malick, A.D. Rabuck, K. Raghavachari, J.B. Foresman, J.V. Ortiz, Q. Cui, A.G. Baboul, S. Clifford, J. Cioslowski, B.B. Stefanov, G. Liu, A. Liashenko, P. Piskorz, I. Komaromi, R.L. Martin, D.J. Fox, T. Keith, M.A. Al-Laham, C.Y. Peng, A. Nanayakkara, M. Challacombe, P.M.W. Gill, B. Johnson, W. Chen, M.W. Wong, C. Gonzalez, J.A. Pople, Gaussian 03, Revision B. 04, Gaussian, Inc., Pittsburgh, PA, 2003.
[24] M.W. Schmidt, K.K. Baldridge, J.A. Boatz, S.T. Elbert, M.S. Gordon, J.H. Jensen, S. Koseki, N. Matsunaga, K.A. Nguyen, S.J. Su, T.L. Windus, M. Dupuis, J.A. Montgomery Jr., J. Comput. Chem. 14 (1993) 1347–1363.
[25] R.V. Williams, Chem. Rev. 101 (2001) 1185–1204.
[26] Z. Chen, C.S. Wannere, C. Corminboeuf, R. Puchta, P.v.R. Schleyer, Chem. Rev. 105 (2005) 3842–3888.
[27] A.J. Wurzer, T. Wilhelm, J. Piel, E. Reidle, Chem. Phys. Lett. 299 (1999) 296–302.
[28] S. Klein, M.J. Bearpark, B.R. Smith, M.A. Robb, M. Olivucci, F. Bernardi, Chem. Phys. Lett. 292 (1998) 259–266.